

Review

# Pt-Ni and Pt-M-Ni (M = Ru, Sn) Anode Catalysts for Low-Temperature Acidic Direct Alcohol Fuel Cells: A Review

Ermete Antolini

Scuola di Scienza dei Materiali, Via 25 aprile 22, Cogoleto, 16016 Genova, Italy; ermantol@libero.it;  
Tel.: +39-3703101994

Academic Editor: Francesco Lufrano

Received: 21 November 2016; Accepted: 22 December 2016; Published: 1 January 2017

**Abstract:** In view of a possible use as anode materials in acidic direct alcohol fuel cells, the electro-catalytic activity of Pt-Ni and Pt-M-Ni (M = Ru, Sn) catalysts for methanol and ethanol oxidation has been widely investigated. An overview of literature data regarding the effect of the addition of Ni to Pt and Pt-M on the methanol and ethanol oxidation activity in acid environment of the resulting binary and ternary Ni-containing Pt-based catalysts is presented, highlighting the effect of alloyed and non-alloyed nickel on the catalytic activity of these materials.

**Keywords:** direct methanol fuel cells; direct ethanol fuel cells; Pt-Ni; methanol oxidation; ethanol oxidation

## 1. Introduction

Low-temperature direct alcohol fuel cells (DAFCs), in particular those using methanol (direct methanol fuel cell, DMFC) or ethanol (direct ethanol fuel cell, DEFC) as the liquid fuel have been the subject of considerable attention in the last decades. DAFCs are an important alternative power source for many applications, particularly as portable devices. The use of organic liquid fuels has advantageous features including easy and safe handling, storage and transportation, high energy density and low cost [1–4]. However, despite these advantages, DAFCs are characterized by a significantly lower power density and lower efficiency than the commonly used hydrogen-fuelled polymer electrolyte membranes fuel cells (PEMFCs) because of the slow alcohol oxidation kinetics and alcohol crossover from the anode to the cathode [1–4].

Platinum is the best monometallic catalyst for methanol and ethanol oxidation in acid environments, so it is commonly used as an anode catalyst in low-temperature fuel cells, but the high cost of platinum and its poisoning by strongly adsorbed species coming from the dissociative adsorption of the alcohols are a major drawback for the commercialization of DAFCs. Efforts to mitigate the poisoning of Pt have been concentrated on the addition of co-catalysts to the platinum [1–4]. The addition of a second metal or a metal oxide as a promoter for the oxidation of adsorbed species is a way to solve the problem of Pt poisoning. In bimetallic catalysts, according to the bifunctional mechanism, Pt can initiate the alcohol oxidation through adsorption-dehydrogenation steps and the second metal or metal oxide can supply the oxygen species, needed to oxidize the adsorbed species and liberate the Pt surface for further alcohol adsorption/oxidation [5,6]. According to the ligand or the electronic effect, the second metal modifies the electronic properties of the Pt by charge transfer processes and lowers the adsorption energy of alcohol oxidation intermediate species onto the Pt surface [5,7,8]. A broad variety of bimetallic catalysts, such as Pt-Ru, Pt-Sn, Pt-Ni, Pt-Co, Pt-W and Pt-Mo, were investigated to replace the monometallic Pt catalysts [9]. Among them, Pt-Ru and Pt-Sn catalysts showed a considerable improving of the electrocatalytic activity for the methanol

oxidation reaction (MOR) and the ethanol oxidation reaction (EOR), respectively, but they presented unsatisfactory stability in fuel cell environment [10,11]. Among bimetallic systems, besides a fair catalytic activity for alcohol oxidation, Pt-Ni has the promising characteristics of being resistant to dissolution in the potential range used for alcohol electrooxidation, likely due to either the stability of Ni in the Pt lattice or a passivating role of Ni hydroxides [12]. A dissolution of the co-catalyst is observed, instead, in various bimetallic catalyst systems like Pt-Ru [10] and Pt-Sn [11]. Another advantage of the use of nickel as the second metal in binary Pt-based catalysts is due to its low cost in comparison to Ru which is a precious metal.

In this work an overview of the methanol and ethanol oxidation in acid environment on binary Pt-Ni and ternary Ni-containing Pt-based catalysts is presented, highlighting the effect of alloyed and non-alloyed nickel on the catalytic activity of these materials.

## 2. Structural Characteristics of Pt-Ni Catalysts

In the Pt-Ni system, there are four stable phases, that is, the disordered fcc solid solution phase, and the ordered phases Pt<sub>3</sub>Ni, PtNi and PtNi<sub>3</sub> [13]. The Pt<sub>1-x</sub>Ni<sub>x</sub> (0 < x < 1) alloys form solid solutions (A1 phase, space group: Fm-3m) at all concentrations, with Pt and Ni atoms randomly distributed in all crystallographic sites [14]. The structures of ordered PtNi<sub>3</sub> and Pt<sub>3</sub>Ni are both L1<sub>2</sub> (space group: Pm-3m), where the roles of Pt and Ni are interchanged, while the structure of ordered PtNi is L1<sub>0</sub>, (space group: P4/mmm). Generally, carbon supported Pt-Ni catalysts commonly used in fuel cells are partially alloyed, formed by a mixing of PtNi alloys and Ni oxy/hydroxides.

Platinum tends to segregate on PtNi alloy surface [15]. Wang et al. [16] reported a theoretical approach to predicting surface segregation in nanoparticles by using a modified embedded atom method and Monte Carlo simulations. They calculated the concentrations of Pt atoms in the outermost three atomic layers of four simulated Pt<sub>75</sub>Ni<sub>25</sub> nanoparticles. Pt concentration was nearly 100 at % in the outermost layer of Pt<sub>75</sub>Ni<sub>25</sub> nanoparticles. This theoretical prediction quantitatively agrees with a direct measurement for annealed Pt<sub>75</sub>Ni<sub>25</sub> polycrystal surfaces [17], in which the Pt concentration in the outermost layer was about 50 at % higher than that in the second Ni enriched atomic layer, while Pt concentration in the third atomic layer was about 75 at %. Pt concentration in the second layer of simulated Pt<sub>75</sub>Ni<sub>25</sub> nanoparticles was about 25 at % lower than the overall concentration of 75 at % and increases gradually with nanoparticle size.

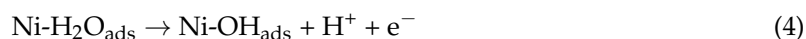
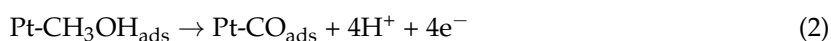
## 3. Methanol Oxidation on Pt-Ni Catalysts

The methanol oxidation is a complex reaction, leading to high overpotentials under fuel cell operating conditions. Among different metals, platinum possess the highest activity for methanol oxidation in acid media, and is commonly used as electrode material in low-temperature fuel cells. The high cost and the limited resources of platinum, however, as well as the low rate of the reaction, boosted the development of binary and ternary Pt-based alloys. Among different Pt-M catalysts, Pt-Ru presented the highest MOR activity, however, as previously reported, high cost and dissolution of Ru in fuel cell environment are serious drawbacks. Pt-Ni bimetallic nanocatalysts have been studied extensively in recent years because of low cost of Ni and the synergistic effect of Pt and Ni, which can improve the performance of the catalysts. Generally, the MOR onset potential on Pt-Ni catalysts is lower than on Pt [18–25] but higher than on PtRu catalysts [18,19,26]. Few works reported a MOR onset potential on Pt-Ni higher [27–29] or similar [30] than that on Pt. The MOR onset potential difference between PtNi and Pt ( $\Delta_{V_{0PtNi}-V_{0Pt}}$ ) and between PtNi and PtRu ( $\Delta_{V_{0PtNi}-V_{0PtRu}}$ ) is reported in Table 1 for some Pt-Ni catalysts. As can be seen in Table 1, the most part of the  $\Delta_{V_{0PtNi}-V_{0Pt}}$  values were in the range from –10 to –100 mV. The increase of the MOR onset potential on Pt-M (M = Ni, Co) alloys with increasing the amount of M alloyed for low M contents reported by Antolini et al. [31] was overall ascribed to the dilution effect of Pt in Pt-M alloys, hindering the methanol adsorption, thus counteracting the positive electronic effect of Ni alloying on the MOR.

**Table 1.** Difference in MOR onset potential between Pt-Ni and Pt ( $\Delta_{V_{O_{PtNi}}-V_{O_{Pt}}}$ ), and between Pt-Ni and Pt-Ru ( $\Delta_{V_{O_{PtNi}}-V_{O_{PtRu}}}$ ) for some Pt-Ni catalysts with various Pt:Ni atomic ratio and prepared by different synthesis methods.

Pt:Ni Atomic Ratio	Characteristics/ Synthesis Method	$\Delta_{V_{O_{PtNi}}-V_{O_{Pt}}}$ (mV)	$\Delta_{V_{O_{PtNi}}-V_{O_{PtRu}}}$ (mV)	Reference
3:1 1:1	NaBH <sub>4</sub> reduction method at room T. Unsupported nanoparticles	−30 −60	+55 +25	[18]
1:1	Carbon supported Pt-Ni	−15 (25 °C) −10 (50 °C) −40 (75 °C)	+70 (25 °C) +55 (50 °C) +30 (75 °C)	[19]
2:1	Few-layered graphene (FLG) supported Pt-Ni. Polyol assisted reduction method	−100	0	[20]
1:1 0.3:1	Self-decorated PtNi alloy nanoparticles, on MWCNT in [BMIm][BF <sub>4</sub> ] ionic liquid	−60 −90		[21]
24:1 6.7:1 3:1 2:1 1:1	Adsorption of nickel laurate on Pt/C followed by reduction at 900 °C in H <sub>2</sub> /N <sub>2</sub> atmosphere	−13 −25 −25 −50 −37		[22]
0.9:1 1.2:1	NiO loaded on Vulcan XC-72R carbon black. Pt was further chemically reduced by sodium borohydride on that NiO/C using the impregnation and the microwave methods. Partially alloyed Pt-Ni	−35 −92		[23]
2:1 1:1	Pt-Ni modified polyindole (Pin) films	−100 −100		[24]
1:1	Electrodeposition of Pt-Ni on MWCNT	−50		[25]
3:1	Synthesis of PtNi/CNT by chemical oxidation of CNTs, two-step refluxing and subsequent hydrogen reduction	+20		[27]
2.3:1	Carbon supported Pt-Ni	+65		[28]
2:1 1.5:1 1:1	Carbon supported Pt-Ni	+100 +100 +100		[29]
2.3:1	Pt and Pt <sub>0.7</sub> Ni <sub>0.3</sub> disc electrodes with a diameter of 12 and 2 mm in thickness	0		[30]

The effect of the addition of nickel to platinum on the electrooxidation reaction of methanol can be mainly explained by the bifunctional mechanism and the electronic interaction between Ni and Pt. Moreover, nickel oxyhydroxides present in Pt-Ni catalysts can act not only as a promoter of Pt but also as a catalyst capable of oxidizing methanol in acid solution [32]. Furthermore, these mixed oxides, beside their corrosion resistance and stability under methanol oxidation conditions, provide mixed protonic and electronic conductivity which may facilitate the charge transfer during the oxidation process. According to the bifunctional mechanism, the methanol electro-oxidation mechanism at Pt-Ni catalysts takes place in the following way [33]:



Dissociative adsorption of methanol occurs on platinum, then the oxidation of the strongly adsorbed oxygen-containing species is facilitated in the presence of a second metal, in this case Ni, capable of activating H<sub>2</sub>O at a lower potential than that accomplished by pure Pt, by supplying

oxygen atoms at an adjacent site. Also Ni oxy/hydroxides (NiO, Ni(OH)<sub>2</sub> and NiOOH) could provide Ni-OH<sub>ads</sub> to remove CO<sub>ads</sub> from Pt active sites [32].

Various investigations, based on the modification of the electronic structure of Pt, have been devoted to explore the mechanism of the increased activity of Pt-Ni catalysts for methanol oxidation. When alloyed with Pt, Ni induces charge transfer from Ni to Pt, thus modifying the electronic structure of Pt and giving rise to a lower density of states at Fermi level [18]. Density functional theory (DFT) was used to explain the MOR activity enhancement by addition of Ni to Pt [34,35]. The structure and reactivity of Pt<sub>(7-x)</sub>Ni<sub>x</sub> ( $x = 1, 2, 3$ ) clusters derived from the coupled tetragonal pyramid (CTP) structure of Pt<sub>7</sub> have been studied using DFT calculations [34]. Pt<sub>5</sub>Ni<sub>2</sub>, which is most stable among the various isomers of Pt<sub>(7-x)</sub>Ni<sub>(x)</sub> ( $x = 1, 2, 3$ ) clusters, was selected as the model for methanol decomposition on PtNi bimetallic catalyst. The reaction pathways for methanol dehydrogenation on Pt<sub>7</sub> and Pt<sub>5</sub>Ni<sub>2</sub> clusters and the enhancement of the MOR activity of PtNi cluster have been investigated. The methanol dehydrogenation on Pt<sub>7</sub> cluster preferentially takes place through C-H bond breaking, while on Pt<sub>5</sub>Ni<sub>2</sub> the pathway starting from O-H bond scission is more appropriate. Moreover, the complete dehydrogenation product of methanol, CO, dissociates more preferable on Pt<sub>5</sub>Ni<sub>2</sub> cluster than that on Pt<sub>7</sub>. Through the analysis of electronic structure, it was inferred that the modification of Pt electronic structure likely offset the electron transfer from CO 5σ orbital to Pt and reduces the CO poisoning. To simulate the experimental cases, in DFT calculations Xu et al. [35] used Pt<sub>2</sub>M (111) slabs with pure Pt surface. The d-band center of Pt shifted to a lower value after the incorporation of Co or Ni, in agreement with the results of Stamenkovic et al. obtained using a Pt<sub>3</sub>M model [36]. The downshift of d-band center relative to the Fermi level gives rise to the decrease of the electron back-donation from the Pt 5d orbital to the 2p\* orbital of CO, thus weakening the Pt-CO bonding.

As a direct comparison of the electrochemical properties of Pt-Ni catalysts is not correct, being catalyst from different datasets prepared by different methods and supported on different substrates, to remove other effects than the nickel amount, comparison was carried out on the  $A_{Pt-Ni}/A_{Pt}$  ratio, where  $A_{Pt-Ni}$  and  $A_{Pt}$  are the electrochemical characteristics of Pt-Ni and Pt catalysts prepared in the same way and supported on the same substrate. The dependence of the Pt-Ni to Pt electrochemically active surface area ( $ECSA_{Pt-Ni}/ECSA_{Pt}$ ), MOR specific activity ( $SA_{Pt-Ni}/SA_{Pt}$ ) and mass activity ( $MA_{Pt-Ni}/MA_{Pt}$ ) ratios in acid media on Ni content in the Pt-Ni catalysts with various alloying degrees from different datasets [20–22,37–44] is shown in Figure 1a–c, respectively. As can be seen in Figure 1a the  $ECSA_{Pt-Ni}/ECSA_{Pt}$  vs. Ni data are somewhat dispersed. The scattering of the ECSA data is likely due to counteracting effects, that is, platinum segregation on Pt-Ni alloy surface and, somewhat, a particle size decrease with increasing both alloyed and non-alloyed Ni content [23,40,45,46], increasing the ECSA, and the presence of Ni oxides, decreasing the ECSA. On the one hand, Pt segregation allows the achievement of a high number of Pt active sites on the surface also for high Ni contents in the catalyst, and the addition of Ni species to the system seems to prevent, particle aggregation. On the other hand, a portion of the PtNi nanoparticle surface is covered by nickel oxides. Thus, the resulting effect of Ni content on the ECSA depends on the alloying degree, that is, at a fixed Ni content, as higher is the alloying degree as higher is the ECSA value. As can be seen in Figure 1a, in a rough approximation, the data can be divided in two groups, that is, in one series the data increase with increasing Ni content (dashed line, corresponding to a high alloying degree and a low content of nickel oxide), and in the other they decrease with increasing the amount of Ni (dotted line, related to a high nickel oxide content). Unlike the data of Figure 1a, the  $SA_{Pt-Ni}/SA_{Pt}$  vs. Ni data are more connected (Figure 1b), and the  $SA_{Pt-Ni}/SA_{Pt}$  ratio increases with increasing Ni content in the binary catalysts. In this case alloyed and non-alloyed Ni has a similar positive effect on SA. As can be seen in Figure 1c, the  $MA_{Pt-Ni}/MA_{Pt}$  vs. Ni data are less dispersed than those of Figure 1a

and less gathered than those of Figure 1b. This result is reasonable, considering that MA depends on both SA and ECSA as the following relation:

$$MA = ECSA * SA \quad (6)$$

As expected, MA increases with Ni content in the catalyst. The ratio between the peak current in the forward ( $I_f$ ) and the backward scan ( $I_b$ ) is usually taken as the measure for the tolerance of the catalyst against poisoning by adsorbed species coming from the dissociative methanol adsorption, a higher  $I_f/I_b$  ratio indicating higher tolerance. The dependence of the Pt-Ni to Pt  $I_f/I_b$  ratio ( $I_f/I_b^{Pt-Ni}/I_f/I_b^{Pt}$ ) from different datasets [38,40–44] is shown in Figure 1d: the  $I_f/I_b^{Pt-Ni}/I_f/I_b^{Pt}$  data vs. Ni content are scattered, but they slightly increase with increasing Ni content, that is, the poisoning tolerance slight increases with increasing Ni content in Pt-Ni. In a rough approximation we can separate the data in two groups, each showing an almost linear dependence of  $I_f/I_b^{Pt-Ni}/I_f/I_b^{Pt}$  on Ni content, one related to electronic effects of alloyed Ni (higher  $I_f/I_b^{Pt-Ni}/I_f/I_b^{Pt}$  values, dashed line), and the other to Ni oxide effects (lower  $I_f/I_b^{Pt-Ni}/I_f/I_b^{Pt}$  values, dotted line, in this group the values related to poor alloyed Ni [42,43] are present) on the poisoning tolerance. Thus, it seems that the Pt-Ni electronic interaction dominates the promoting effect of Ni on adsorbed CO oxidation by weakening the Pt-CO bonding energy rather than the bifunctional mechanism related to Ni oxides. In some cases, ECSA, SA, MA and  $I_f/I_b$  of Pt are higher than those of Pt-Ni. Figure 1e shows the histogram of  $(A_{PtNi}/A_{Pt})_{<1} / (A_{PtNi}/A_{Pt})_{Tot}$  ratios for A = ECSA, SA, MA and  $I_f/I_b$ , where  $(A_{PtNi}/A_{Pt})_{Tot1}$  and  $(A_{PtNi}/A_{Pt})_{<1}$  are the number of values of the ratio total and lower than 1, respectively. The highest value of these ratios was observed for the ECSA (27%). In the other cases the value of the ratios was around 10%. However, the value of the ratio for A = ECSA depends on the Ni content in the catalyst, that is, for Ni < 30 at % was 9% and for Ni > 30 at % was 40%: the considerably higher value of the ratio for Ni > 30 at % has to be ascribed to the negative effect on the ECSA of high amounts of Ni oxides.

Up to now, the effect of alloyed and non-alloyed Ni on the electrochemical parameters of the Pt-Ni catalysts was not enough evaluated. The effect of the lattice parameter, that is, of the alloying degree, on the  $SA_{Pt-Ni}/SA_{Pt}$  and  $I_f/I_b^{Pt-Ni}/I_f/I_b^{Pt}$  atomic ratios of Pt-Ni (1:1) catalysts from different datasets [22,41–43,47] is shown in Figure 2. The  $SA_{Pt-Ni}/SA_{Pt}$  ratio goes to a maximum at an intermediate degree of alloying, corresponding to a Ni content in the alloy of ca. 35 at %, and indicating that the specific activity of a partially alloyed catalysts is higher than that of non-alloyed and fully alloyed Pt-Ni (1:1) catalysts. The higher MOR activity of partially alloyed Pt-Ni catalysts than that of non-alloyed and fully alloyed Pt-Ni can be explained by a synergic effect of alloyed and non-alloyed nickel: alloyed Ni promotes methanol dehydrogenation, and non-alloyed Ni facilitates the removal of CO adsorbed species. Conversely,  $I_f/I_b^{Pt-Ni}/I_f/I_b^{Pt}$  increases with increasing the alloying degree, attesting a higher poisoning tolerance of alloyed than non-alloyed Pt-Ni catalysts, and confirming the results of Figure 1d. Regarding the effect of non-alloyed Ni, such as NiO, Ni(OH)<sub>2</sub> and NiOOH, on the MOR activity, Antolini et al. [48] observed an increase in the DMFC performance with increasing the amounts of non-alloyed Ni in the Pt-Ni/C anode electrocatalysts from 5 to 25 at %, with the current normalized both to the Pt mass and the ECSA, for a Ni composition in the alloy around 7 at %. The effect of non-alloyed Ni content, at a Pt:Ni atomic ratio in the alloy of 4:1, on the ECSA, SA and MA of graphene supported Pt-Ni catalysts was reported by Luo et al. [42]. As can be seen in Figure 3,  $SA_{Pt-Ni}/SA_{Pt}$  increased with increasing the non-alloyed Ni/Pt atomic ratio by the increase of the amount of NiO, NiOOH, and Ni(OH)<sub>2</sub> species around Pt atoms, facilitating the removal of CO<sub>ads</sub> species. Conversely, ECSA decreased with increasing non-alloyed Ni due to a decrease of the active surface area by the increasing blocking of active Pt sites by nickel oxy/hydroxide species. As the negative effect of non-alloyed Ni in this range of compositions on the ECSA is more important than the positive effect on the SA, the resulting MA decreased with increasing non-alloyed Ni. From the results of the effect of alloyed and non-alloyed Ni on the SA of Pt-Ni reported in Figures 2 and 3, it results that for compositions higher than 35 at %, the optimal specific activity is attained by a partially alloyed catalyst, with 35 at % Ni alloyed and the rest non-alloyed. However, considering that the ECSA

decreases with increasing the amount of Ni oxides, the optimum alloying degree for the mass activity can be different than the optimum alloying degree for the SA.

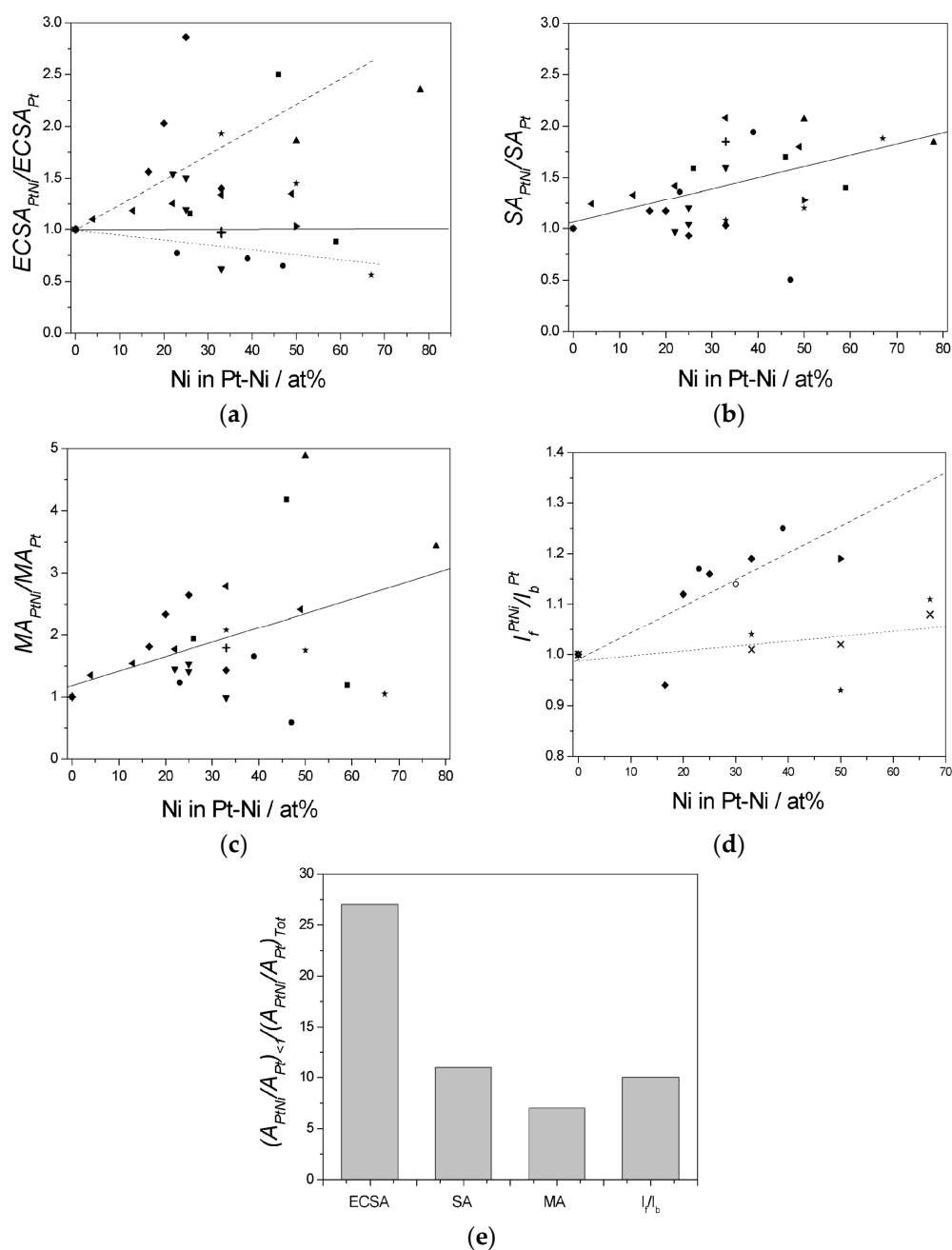


**Figure 1.** Dependence of the Pt-Ni to Pt electrochemically active surface area ( $ECSA_{Pt-Ni}/ECSA_{Pt}$ ) (a); MOR specific activity ( $SA_{Pt-Ni}/SA_{Pt}$ ) (b); MOR mass activity ( $MA_{Pt-Ni}/MA_{Pt}$ ) (c) and ( $I_f/I_b^{Pt-Ni}/I_f/I_b^{Pt}$ ) (d) ratios in acid media on Ni content in Pt-Ni catalysts with various alloying degrees by different datasets; Histogram of  $(A_{Pt-Ni}/A_{Pt})_{<1} / (A_{Pt-Ni}/A_{Pt})_{Tot}$  ratios ( $A = ECSA, SA, MA$  and  $I_f/I_b$ ), where  $(A_{Pt-Ni}/A_{Pt})_{Tot1}$  and  $(A_{Pt-Ni}/A_{Pt})_{<1}$  are the number of values of the ratio total and lower than 1, respectively (e). Symbols in Figure 1a–d: (+) Shen et al. [20]; ( $\blacktriangle$ ) Zhou et al. [21]; ( $\blacktriangleleft$ ) Agrawal et al. [22]; ( $\blacksquare$ ) Wang et al. [37]; ( $\bullet$ ) Jiang et al. [38]; ( $\blacktriangledown$ ) Nassr et al. [39]; ( $\blacklozenge$ ) Hao et al. [40]; ( $\blacktriangleright$ ) Wang et al. [41]; (\*) Luo et al. [42]; (X) Hu et al. [43]; (O) Zhou et al. [44].

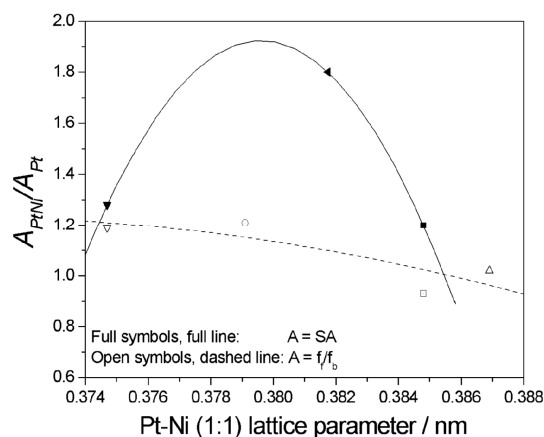


**Figure 2.** Dependence of the Pt-Ni to Pt MOR specific activity ( $SA_{Pt-Ni}/SA_{Pt}$ ) and  $I_f/I_b^{Pt-Ni}/I_f/I_b^{Pt}$  ratios in acid media on fcc lattice parameter of Pt-Ni (1:1) catalysts. (◀) Agrawal et al. [22]; (▼) Wang et al. [41]; (■) Luo et al. [42]; (Δ) Hu et al. [43]; (O) Li et al. [47].

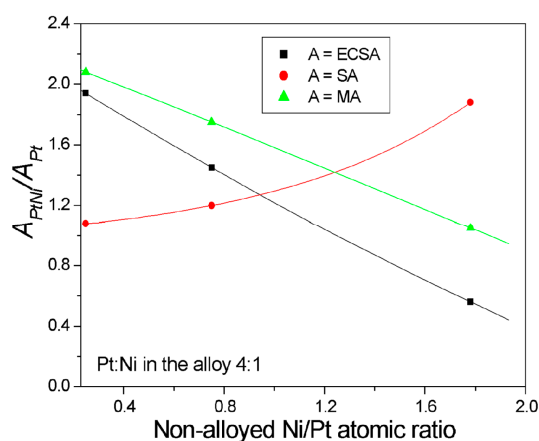


**Figure 3.** Dependence of the ( $A_{Pt-Ni}/A_{Pt}$ ) ratios ( $A = ECSA, SA$  and  $MA$ ) of graphene supported Pt-Ni catalysts on non-alloyed Ni content, at a Pt:Ni atomic ratio in the alloy of 4:1. Data from Reference [42].

#### 4. Ethanol Oxidation on Pt-Ni Catalysts

Due to the presence of a C-C bond, the complete oxidation of ethanol to  $CO_2$  is more complicated than that of methanol. The mechanism of the ethanol oxidation reaction in an acid solution may be described by the following parallel reactions:



The formation of  $CO_2$  goes through two adsorbed intermediates  $C_{1ads}$  and  $C_{2ads}$ , representing fragments with one and two carbon atoms, respectively. C-C bond cleavage represents a major problem in ethanol electrocatalysis [3]. Moreover, platinum is poisoned by strongly adsorbed ethanol oxidation intermediate species [3]. Efforts to reduce Pt poisoning have been addressed to the addition of co-catalysts, particularly ruthenium and tin, to platinum. Conversely to the methanol oxidation, the best binary catalyst for ethanol oxidation in acid environment is not Pt-Ru but Pt-Sn [3]. As in the case of the methanol oxidation, the enhanced EOR activity of these binary catalysts than that of bare Pt was attributed to the bifunctional effect and to the electronic interaction between Pt and alloyed metals. C-C bond cleavage on Pt, however, is hindered by Sn presence in both alloyed and non-alloyed catalysts. To overcome this drawback, binary and ternary Pt-based electrocatalysts have

been investigated. Compared to the MOR, few works reported the ethanol oxidation on Pt-Ni catalysts in acid media [20,46,49–52], the most part as support data in papers addressed to the study of the EOR on ternary Ni-containing catalysts. The dependence of the Pt-Ni to Pt specific activity ( $SA_{Pt-Ni}/SA_{Pt}$ ) and mass activity ( $MA_{Pt-Ni}/MA_{Pt}$ ) ratios in acid media on Ni content in the Pt-Ni catalysts with various alloying degrees by different datasets [20,46,49–51] is shown in Figure 4a,b. The ( $SA_{Pt-Ni}/SA_{Pt}$ ) ratio increased with increasing Ni content in the catalysts (Figure 4a). While taking into account of the few data for the EOR, the slope of ( $SA_{Pt-Ni}/SA_{Pt}$ ) vs. Ni content plot ( $0.028 \text{ at } \%^{-1}$ ) is considerably higher than that for the methanol oxidation ( $0.010 \text{ at } \%^{-1}$ ), indicating that the addition of nickel to Pt is more effective for the EOR than for the MOR. As can be seen in Figure 4b, also the ( $MA_{Pt-Ni}/MA_{Pt}$ ) ratio increases with increasing Ni content in the catalyst. The effect of non-alloyed Ni content on the ECSA, SA and MA of Pt-Ni/C catalysts was reported by Comignani et al. [46]. The dependence of the ( $A_{Pt-Ni}/A_{Pt}$ ) ratios ( $A = \text{ECSA, SA and MA}$ ) of non-alloyed Pt-Ni/C on Ni content in the catalysts is shown in Figure 5. As can be seen in Figure 5, the ( $SA_{Pt-Ni}/SA_{Pt}$ ) ratio increased with increasing Ni content in the catalysts, by the increase of the amount of NiO, NiOOH, and Ni(OH)<sub>2</sub> species. Likely, nickel oxide species promote the activation of both the C-H and O-H bonds of ethanol through oxygen-containing species adsorbed on NiO molecules and the change in the density of states near the Fermi level on the Pt surface atoms, but not the C-C bond cleavage.

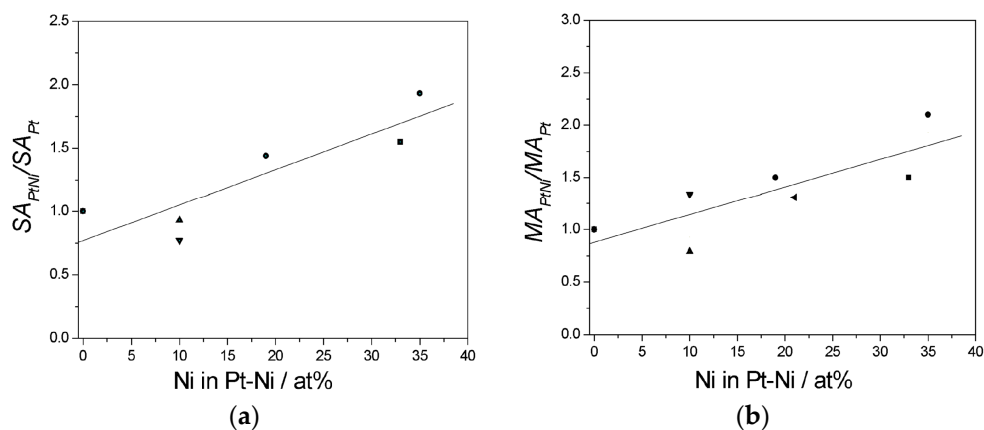


**Figure 4.** Dependence of the Pt-Ni to Pt EOR specific activity ( $SA_{Pt-Ni}/SA_{Pt}$ ) (a) and mass activity ( $MA_{Pt-Ni}/MA_{Pt}$ ) (b) ratios in acid media on Ni content in Pt-Ni catalysts with various alloying degrees by different datasets. (■) Shen et al. [20]; (●) Comignani et al. [46]; (◄) Wang et al. [49]; (▲) Beyhan et al. [50]; (▼) Cantillo et al. [51].

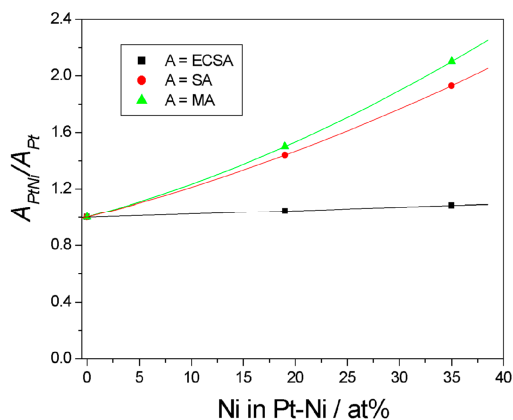


**Figure 5.** Dependence of the ( $A_{Pt-Ni}/A_{Pt}$ ) ratios ( $A = \text{ECSA, SA and MA}$ ) of non-alloyed Pt-Ni/C on Ni content in the catalysts. Data from Reference [46].

Therefore, nickel oxide species seems to act as an oxygen supplier at the interface between Pt and oxide nanoparticles. In this case, the ECSA increased with increasing Ni content in the catalyst, due to the prevailing positive effect of the decrease of particle size with the increase of Ni amount in the catalyst. Thus, also the resulting MA increased with increasing Ni content.

## 5. Stability of Pt-Ni Catalysts in Fuel Cell Environment

### 5.1. General Overview

Generally, the formation of a Pt skin on the surface of Pt-Ni catalysts for a nickel content < 65 at % Ni hinders the dissolution of bulk Pt and Ni atoms. Regarding Pt dissolution, the high corrosion resistance of the Pt skin formed on the surface of Pt<sub>3</sub>M (M = Fe, Co, and Ni) catalysts was explained by Greeley and Norskov by first-principles calculations [53]. They found that the dissolution potential of Pt in Pt “skin” layers from Pt<sub>3</sub>M bulk alloys increased by 0.19, 0.16, and 0.14 V for Pt<sub>3</sub>Fe, Pt<sub>3</sub>Co, and Pt<sub>3</sub>Ni, respectively, with respect to the dissolution potential of pure Pt.

The stability of Pt-based acidic fuel cell catalysts can be considered in two regards: active surface area decrease, due to sintering, and transition metal dissolution under the operating conditions. For this purpose, two main accelerated durability tests (ADTs) were used, that is, (1) acid immersion and (2) repetitive potential cycling (RPC).

### 5.2. Acid Immersion

The test in acid can be carried by a simple immersion of the catalyst in an acid solution (chemical test) or by immersion of the sample in an acid solution at a constant potential (electrochemical test). Park et al. [18] observed no appreciable Ni dissolution from a Pt-Ni(1:1) catalyst in a H<sub>2</sub>SO<sub>4</sub> solution in the potential range of methanol oxidation (0–1.6 V vs. NHE). In various tests Ni loss was observed only on the catalyst surface, giving rise to the formation of a protective Pt-enriched layer [54–57]. A durability chemical test at low pH and 80 °C on Pt<sub>1-x</sub>Ni<sub>x</sub> (0 < x < 1) catalysts, prepared by sputtering Pt and Ni onto thin films of nanostructured whisker-like supports, was performed by Bonakdarpour et al. [54]. For values of x < 0.6, no substantial changes in the lattice size were observed upon dissolution of Ni, indicating that the dissolved nickel metal originated from the surface. However, for electrocatalysts with x > 0.6, the lattice constant increased, indicating that nickel atoms dissolved also from the bulk, and attesting the absence of a protective Pt skin on the surface for high Ni contents. Tests in PEMFCs operating at 80 °C were in good agreement with the chemical test. Hoshi et al. [55] investigated the dissolution of unsupported arc-melted equimolar Pt-M (M: Cu, Co, Ni, Fe) alloys by 3-h immersion tests in a H<sub>2</sub>SO<sub>4</sub> solution at 25 °C. The results indicated that the surfaces of these alloys were covered with a Pt-enriched layer due to preferential dissolution of M atoms. They carried out also an electrochemical test in acid solution under potentiostatic conditions at 1.0, 1.2 and 1.4 V vs. standard hydrogen electrode (SHE) for 1 h. When the Pt-Ni alloy was held at 1.0 and 1.2 V for 1 h, the dissolution rate of Ni was not higher than that under the steady state in the immersion test. The dissolution of Ni at 1.4 V was markedly greater than that at 1.0 and 1.2 V. In a first work, Colon-Mercado et al. [56] carried out ADTs on a commercial Pt<sub>3</sub>Ni/C alloy catalyst by immersion in a H<sub>2</sub>SO<sub>4</sub> solution at a fixed potential between 0.9 and 0.4 V vs. SHE. The effect of ADT on particle size of Pt/C and Pt<sub>3</sub>Ni<sub>1</sub>/C catalysts was evaluated by transmission electron microscopy (TEM) measurements. The Pt<sub>3</sub>Ni<sub>1</sub>/C alloy, due to anchor effects in its structure, showed higher sintering resistance than Pt/C. The mobility of platinum on a carbon surface was hindered in the presence of Ni, thus lowering the sintering rate of Pt atoms. Ni loss took place during ADT, and the total amount of Ni dissolved increased from 8.3% to 12% by increasing the potential from 0.4 to 0.9 V vs. SHE. After the ADT at 0.68 V vs. SHE, despite a 10% loss of Ni, the XRD pattern showed negligible change compared to fresh Pt<sub>3</sub>Ni<sub>1</sub>/C, indicating that Ni loss occurs only on the catalyst surface. In a next work, Colon-Mercado and Popov [57] evaluated the durability of commercial Pt/C and Pt-M/C (M = Ni, Co, Fe and V) alloy catalysts by the same ADT used in their previous work [56]. At 0.8 V vs. NHE, a fast dissolution of

M atoms occurred in the first times of the test, then M loss took place more slowly. The metal loss in the catalysts with a Pt to non-noble metal ratio of 3:1 was lower than that in the catalysts with 1:1 Pt/M ratio. Among the different M, for both 3:1 and 1:1 Pt/M ratio, Pt-Ni alloys showed the lowest metal dissolution. Regarding the stability of non-alloyed Ni, conflicting results have been reported [46,58]. Zignani et al. [58] submitted carbon supported poorly alloyed (Ni atomic fraction in the alloy about 0.05) Pt-Ni (1:1) catalysts to durability tests in a H<sub>2</sub>SO<sub>4</sub> solution at a constant potential (0.8 V vs. RHE) for 30 h. Following the stability test, the Ni EDX composition (total Ni in the catalyst) was near the same than the Ni XRD composition (Ni alloyed), indicating that the almost all non-alloyed Ni was lost. Comignani et al. [46] investigated the stability of Pt-NiO/C catalysts in a 0.5 M H<sub>2</sub>SO<sub>4</sub> + 1 M ethanol solution by potentiostatic experiments for 12 h at 0.6 V and 60 °C. By a ICP analysis of the solution, the absence of nickel ions indicated that nickel oxide nanoparticles are stable to corrosion in acidic media.

### 5.3. Repetitive Potential Cycling (RPC)

Repetitive potential cycling is a widely used technique to evaluate the stability of a catalyst. Generally, the ageing test by repetitive potential cycling is more severe than under steady-state conditions [59]. In the case of platinum alloys, both the non-noble metal particles and Pt dissolve into the electrolyte. Then the dissolved Pt redeposits on the surface of larger particles (Ostwald ripening), resulting in a Pt surface-enrichment [60]. The stability of the catalysts submitted to RPC essentially depends on the cycle number and potential range, and also on the scan rate.

The stability of Pt-Ni catalysts was evaluated by RPC in different works [55,57,58,61]. Hoshi et al. [55] investigated the dissolution of unsupported arc-melted equimolar Pt-M (M: Cu, Co, Ni, Fe, Pt:M = 1:1) alloys by RPC (100 cycles) on the Pt-enriched layer obtained by immersion of Pt-M catalysts in a H<sub>2</sub>SO<sub>4</sub> solution at 100 mV·s<sup>-1</sup> between 0.0 V and 1.4 V. The M dissolution was more significant under potential cycling than by potentiostatic polarization at 1.4 V, indicating that the inhibition due to the Pt-enriched layer did not occur under potential cycling between 0 and 1.4 V. Colon-Mercado and Popov [57] evaluated the durability of Pt/C and Pt-M/C (M = Ni, Co, Fe and V, Pt:M 3:1 and 1:1) catalysts by RPC in a H<sub>2</sub>SO<sub>4</sub> solution at a scan rate of 5 mV·s<sup>-1</sup> in a potential range of 0.03–1.24 V vs. NHE for 1100 cycles. In the case of binary catalysts, both the non-noble metal particles and Pt dissolved into the electrolyte. Then the dissolved Pt redeposits on the surface of larger particles. After 1000 cycles, the highest loss of surface area (~57%) from the pure platinum catalyst indicated that the processes of Ostwald ripening, Pt particle migration and sintering occur at a higher rate when compared to the redeposition and particle sintering of Pt-M/C catalysts. The lowest surface area loss (~43%) was observed for the catalysts with a non-noble metal content of 25 at % (Pt<sub>3</sub>Co<sub>1</sub>/C and Pt<sub>3</sub>Ni<sub>1</sub>/C). Zignani et al. [58] submitted a Pt-Ni/C (1:1) poorly alloyed (Ni atomic fraction in the alloy about 0.05) catalyst to repetitive potential cycling in a H<sub>2</sub>SO<sub>4</sub> solution (1000 cycles between 0.5 and 1.0 V vs. RHE at 20 mV·s<sup>-1</sup>). Following RPC, the Pt/Ni atomic ratios by both XRD (Ni alloyed) and EDX (Ni total) were higher than those before cycling. Moreover, the Pt/Ni atomic ratio by XRD was lower than Pt/Ni by EDX, meaning that the amount of non-alloyed Pt was higher than that of non-alloyed Ni. The loss of all non-alloyed Ni and dissolution of part of the Pt–Ni alloy, with reprecipitation of Pt (but not of Ni) on the catalyst surface likely occurred. To evaluate the effect of the transition from the disordered alloy phase to the ordered intermetallic phase on the durability, disordered (D-PtNi/C) and ordered (O-PtNi/C) PtNi/C catalysts were submitted to a RPC [61]. After cycling, the Pt:Ni atomic ratio changed from 1:1 to approximately 3.2:1 and 1.4:1 for the D-PtNi/C and the O-PtNi/C, respectively, indicating that the ordered PtNi intermetallic nanoparticles are more stable than the disordered PtNi alloy, in agreement with the electrochemical results.

## 6. Methanol Oxidation on Ternary Pt-Ru-Ni Catalysts

Also if Pt-Ru catalysts present much higher activity for methanol oxidation than pure Pt, the performance of DMFCs remains considerably lower than that of fuel cells operating in the same conditions but fuelled with hydrogen. Thus, research efforts have been addressed to the improvement of the MOR activity of Pt-Ru catalysts. A way to enhance the MOR activity as well as to reduce the cost of Pt-Ru catalysts is the replacement of part of Pt and/or Ru atoms with a third metal (M), giving rise to the formation of ternary Pt-Ru-M catalysts. Regarding the third metal, some metals fully alloy with Pt, some only partially alloy, and some do not form alloy with Pt. Generally, as higher is the content of the third metal as lower is the degree of alloying and higher is the amount of its oxide [62]. However, as the presence of a third metal influences the amount of Ru alloyed, it is difficult to estimate the degree of alloying of the third component. The formation of a ternary alloy is mainly observed in the Pt-Ru-Ni system [62]. The MOR activity of Pt-Ru-M catalysts was compared in some works [63–66]. In all these papers Pt-Ru-Ni was reported as the best catalyst for the MOR. Fe, Co and Ni were selected as a third metals because the low cost of their precursors, and their effect on PtRu activity for methanol electrooxidation was investigated. [63,64]. Huang et al. [63] observed that the addition of M to Pt-Ru enhances the electrocatalytic properties for methanol oxidation and Pt-Ru-Ni has the best catalytic activity and stability. Jeon et al. [64] found that, among Pt<sub>45</sub>Ru<sub>45</sub>M<sub>10</sub>/C (M = Fe, Co, and Ni) catalysts, the Pt<sub>45</sub>Ru<sub>45</sub>Fe<sub>10</sub>/C and Pt<sub>45</sub>Ru<sub>45</sub>Ni<sub>10</sub>/C catalysts showed the highest mass activity. Regarding the specific activity, the Pt<sub>45</sub>Ru<sub>45</sub>Ni<sub>10</sub>/C catalysts showed the highest activity, 170% higher than that of a commercial Pt-Ru/C catalyst. PtRu and Pt<sub>50</sub>Ru<sub>40</sub>M<sub>10</sub> (M = Ni, Sn and Mo) electrocatalysts were prepared by a NaBH<sub>4</sub> reduction method [65]. The mass activity and specific activity of Pt-Ru-Ni were much higher than that of Pt-Ru and the other ternary catalysts. SA of the Pt-Ru-Ni catalyst was ca. 2.2 times higher than that of Pt-Ru.

The MOR activity of Pt-Ru-Ni catalysts has been widely investigated [12,18,20,26,66–72]. Except for Papaderakis et al. [66], which compared the methanol oxidation on Pt-Ru-Ni and Pt-Ni (this comparison is of little meaning, as it is trivial that the addition of Ru to Pt-Ni increase the MOR activity), in all works a comparison between Pt-Ru-Ni and Pt-Ru catalysts was made, and the MOR activity of Ni-containing catalysts was always higher than that of Pt-Ru. Park et al. [12] studied the methanol oxidation on Pt and partially alloyed Pt-Ni (1:1 and 3:1), Pt-Ru-Ni (5:4:1 and 6:3.5:0.5) and Pt-Ru (1:1) catalysts. Among these catalysts, Pt-Ru-Ni (5:4:1) showed the lowest MOR onset potential. The enhanced oxidation of CO coming from methanol decomposition on Pt-Ru-Ni (5:4:1) was ascribed to the electron transfer from Ru and Ni to Pt and also to the surface redox activity of Ni oxides toward the CO. Liu et al. [67] compared the methanol oxidation on almost non-alloyed Pt-Ru-Ni catalysts of different atomic compositions and on a commercial Pt-Ru alloy catalyst. The onset potential for methanol oxidation on the ternary catalysts was slightly lower than that for the commercial Pt-Ru catalyst. Methanol oxidation current densities decreased in the order of Pt-Ru-Ni(60:30:10)/C > Pt-Ru-Ni(67.5:22.5:10)/C > Pt-Ru-Ni(50:40:10)/C > Pt-Ru/C, indicating that the Ni/(Ru + Ni) atomic ratio of 0.25 was the most effective, in agreement with the results of Wang et al. [68] which investigated the optimum composition of a Pt-Ru-Ni system by a combinatorial method: the Pt-Ru-Ni (60:30:10) catalyst showed the highest activity for methanol oxidation. Martinez-Huerta et al. [69] studied the effect of Ni addition to Pt-Ru/C catalysts on CO and methanol oxidation. They observed that the oxidation state of Ni plays a key role on the catalytic performance of Pt-Ru-Ni/C electrocatalysts, particularly in the CO oxidation reaction, related to the development of Pt–Ni electronic interaction. They also evaluated the influence of the nature of the carbon support on the catalytic activity. Electrocatalysts prepared on a carbon-modified substrate displayed higher activities in the methanol oxidation reaction than those prepared over non-treated carbon. For the Ni-containing samples, the preparation route determines the degree of interaction between Pt and Ni of the different samples and hence their catalytic performance.

For ternary Pt-Ru-Ni catalysts, the dependence of the electrochemical parameters on the Ni/(Ru + Ni) atomic ratio is more interesting than their dependence on the overall Ni content. The dependence of the Pt-Ru-Ni to Pt-Ru MOR specific activity ( $SA_{Pt-Ru-Ni}/SA_{Pt-Ru}$ ) electrochemically active surface area ( $ECSA_{Pt-Ru-Ni}/ECSA_{Pt-Ru}$ ), particle size ( $d_{Pt-Ru-Ni}/d_{Pt-Ru}$ ) and MOR mass activity ( $MA_{Pt-Ru-Ni}/MA_{Pt-Ru}$ ) ratios in acid media on the Ni/(Ru + Ni) atomic ratio by different datasets [20,26,63–65,70,71] is shown in Figure 6a–d. The  $SA_{Pt-Ru-Ni}/SA_{Pt-Ru}$  vs. Ni/(Ru + Ni) plot presents a sharp peak centered at ca. 20 at % (Figure 6a), followed by a slow decrease of the  $SA_{Pt-Ru-Ni}/SA_{Pt-Ru}$  ratio with increasing Ni content, indicating a synergic effect of Ru and Ni on the MOR specific activity in a short Ni/(Ru + Ni) ratio range, centered at ca. 0.2 Ni/(Ru + Ni). This result is reasonable, considering the Ru is a more effective co-catalyst for methanol oxidation in Pt-based binary catalysts than Ni. The dependence of the  $ECSA_{Pt-Ru-Ni}/ECSA_{Pt-Ru}$  ratio on Ni/(Ru + Ni) is more complex (Figure 6b). The data can be interpolated by a parabolic curve of order 3, with a minimum at ca. 15 at % Ni/(Ru + Ni), and a maximum at ca. 70 at % Ni/(Ru + Ni). As all these catalysts are well alloyed, an effect on Ni and Ru oxides on the ECSA should be excluded. Thus, this anomalous behaviour could depend on the effect of Ni content on the particle size: indeed, as can be seen in Figure 6c, for Ni/(Ru + Ni) in the range 0.2–0.6 the particle size decrease with increasing Ni, but for Ru- and Ni-rich catalysts the particle size increases with increasing Ni content.

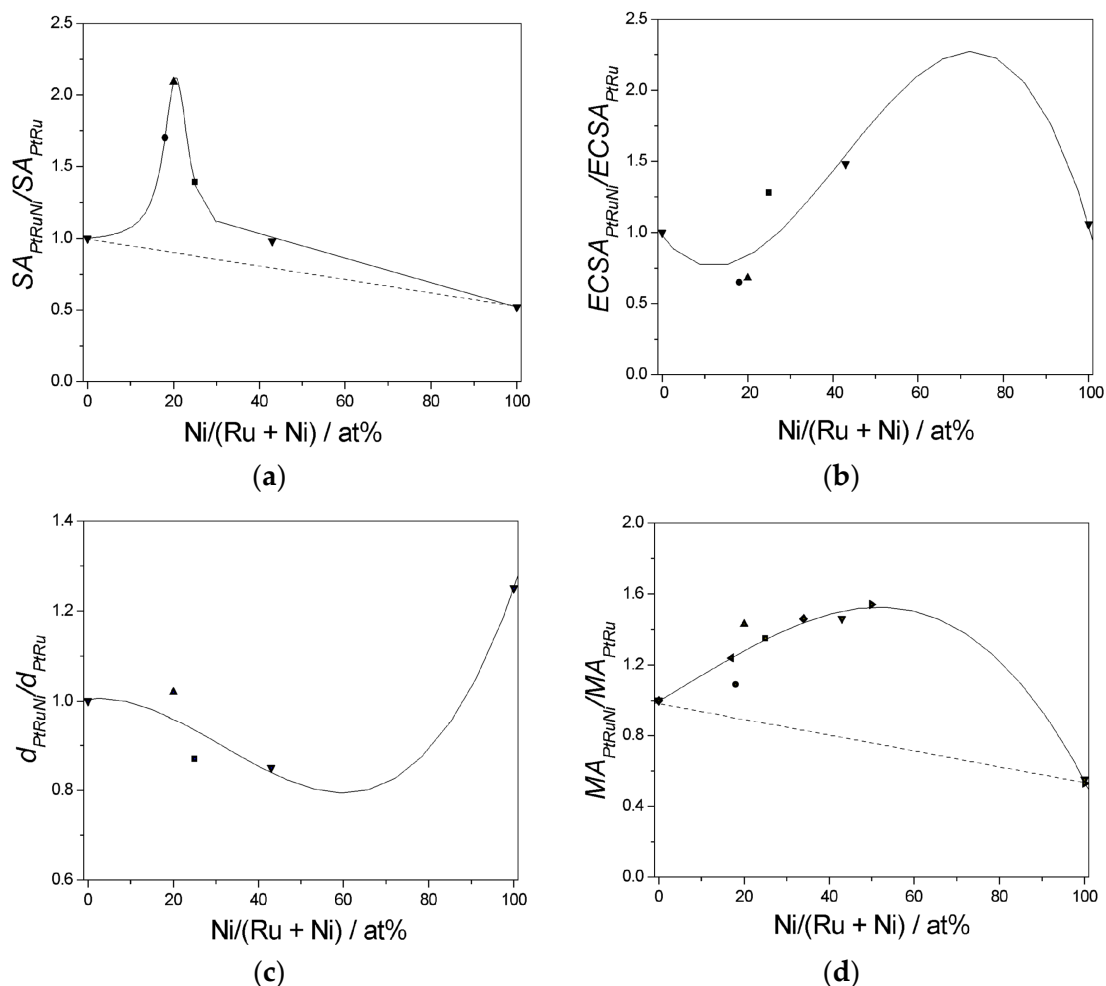
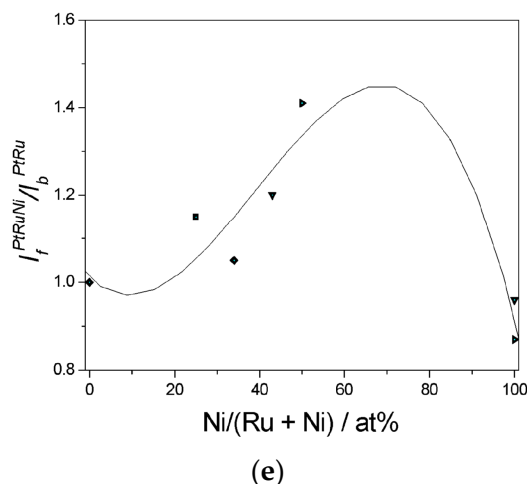


Figure 6. Cont.



**Figure 6.** Dependence of the Pt-Ru-Ni to Pt-Ru EOR specific activity ( $SA_{Pt-Ru-Ni}/SA_{Pt-Ru}$ ) (a); electrochemically active surface area ( $ECSA_{PtRu-Ni}/ECSA_{Pt-Ru}$ ) (b); particle size ( $d_{Pt-Ru-Ni}/d_{Pt-Ru}$ ) (c) EOR mass activity ( $MA_{Pt-Ru-Ni}/MA_{Pt-Ru}$ ) (d) and ( $I_f/I_b^{Pt-Ru-Ni}/I_f/I_b^{Pt-Ru}$ ) (e) ratios in acid media on Ni/(Ru + Ni) atomic ratio in Pt-Ru-Ni catalysts with various alloying degrees by different datasets. (▼) Shen et al. [20]; (►) Zhao et al. [26]; (■) Huang et al. [63]; (●) Jeon et al. [64]; (▲) Kang et al. [64]; (◄) Ye et al. [70]; (◆) Zhao et al. [71].

The resulting  $MA_{Pt-Ru-Ni}/MA_{Pt-Ru}/Ni(Ru + Ni)$  data are well represented by a parabolic curve with a maximum at ca. 45 at % Ni/(Ru + Ni) (Figure 6d). A synergistic effect of Ru and Ni, depending on the Ni/(Ru + Ni) ratio, can be observed. The dependence of the Pt-Ni-Ru to Pt-Ru  $I_f/I_b$  ratio ( $I_f/I_b^{Pt-Ru-Ni}/I_f/I_b^{Pt-Ru}$ ) is shown in Figure 6e: in the same way than  $MA_{Pt-Ru-Ni}/MA_{Pt-Ru}$ , a synergistic effect can be observed, indicating that Ni presence increases the poisoning tolerance of Pt-Ru. An interesting core-shell structured Pt-Ru-Ni catalyst with Ni-rich core and Pt-Ru-rich shell was synthesized on functionalized carbon nanotubes by dealloying and annealing of Pt-Ru-Ni (1:1:1) [72]. Dealloyed Pt-Ru-Ni nanoparticles annealed at 450 °C, with a surface composition of Pt:Ru:Ni = 1.0:1.13:0.24, showed significantly low onset potential and high activity for the MOR, achieving a current density significantly higher than that measured on Pt-Ru-Ni before dealloying and annealing treatment. After polarization for 5000 s at 0.4 V vs. Ag/AgCl, the stable current for the MOR on Pt-Ru-Ni (1.0:1.13:0.24) electrocatalysts was  $34.3 \text{ A} \cdot \text{g}^{-1}_{Pt}$ , considerably higher than  $10.2 \text{ A} \cdot \text{g}^{-1}_{Pt}$  of Pt-Ru-Ni (1:1:1). The enhanced activity and stability was related to the formation of an intermetallic PtRu skinned shell and a Ni rich core structure.

## 7. Ethanol Oxidation on Ternary Pt-Sn-Ni and Pt-Ru-Ni Catalysts

Unlikely for the methanol oxidation, Pt-Sn, and not Pt-Ru, is the best catalyst for ethanol oxidation. Pt-Sn best catalyst for the EOR The addition of tin to platinum increases the activity of Pt towards ethanol oxidation, not enhancing C–C bond breaking to form  $\text{CO}_2$ , but improving the ethanol oxidation to acetaldehyde and acetic acid [73]. Pt-Sn catalysts, however, have unsatisfactory stability in fuel cell environment. To further increase its EOR activity and stability and to promote C–C bond cleavage the addition of a third metal to Pt-Sn has been investigated [74]. Different ternary Pt-Sn-M/C (M = Ni, Co, Rh, Pd) and their corresponding bimetallic Pt-M/C (C = Sn, Ni, Co, Rh, Pd) catalysts were synthesized by the Bönemann's method and their activity for ethanol oxidation was evaluated [74]. Among all these catalysts, Pt-Sn-Ni/C and Pt-Sn-Co/C showed the lowest onset potential for ethanol electrooxidation and the highest peak current densities. Tests of these materials as anode catalysts in direct ethanol fuel cells (DEFCs) confirmed these results: DEFCs with ternary Pt-Sn-Ni/C and Pt-Sn-Co/C catalysts showed considerably higher overall performance and peak power density than those of the cells with Pt-Sn/C and the other ternary catalysts.

Different works were addressed to the ethanol oxidation on Pt-Sn-Ni catalysts [50–52,75–81]. In all these works a comparison between Pt-Sn-Ni and Pt-Sn catalysts was made, and the MOR activity of Ni-containing catalysts was always higher than that of Pt-Sn. The dependence of the Pt-Sn-Ni to Pt-Sn mass activity ( $MA_{Pt-Sn-Ni}/MA_{Pt-Sn}$ ) ratio in acid media on the Ni/(Sn + Ni) atomic ratio by different datasets [50,51,76–80] is shown in Figure 7. A synergic effect between Sn and Ni can be observed with a maximum at a value of the Ni/(Sn + Ni) ratio of ca. 0.35. The presence of Ni seems to promote C–C bond cleavage and facilitate the removal from the catalyst surface of adsorbed intermediates [50,74,81]. By in situ Fourier transform infrared (FTIR) spectroscopy measurements, it was observed that the addition of Ni or Pd to Pt-Sn considerably improves the formation of acetic acid at lower potentials [81]. At higher potentials, instead, the addition of Ni and Rh to Pt-Sn results in a high conversion of ethanol to CO<sub>2</sub>, indicating that these metals can promote C–C bond breaking [81]. Pt-Sn-Ni (3:1:1) and Pt-Ni (3:1) were submitted to accelerated stress tests by repetitive potential cycling (1000 cycles) between 0.05 and 1.0 V vs. RHE at 50 mV·s<sup>-1</sup> in a H<sub>2</sub>SO<sub>4</sub> solution [74]. After the stress test, the solution was analyzed by graphite furnace atomic absorption spectrometry (GF AAS) to quantify the dissolution of Ni: the results indicated that nickel was considerably more stable in the ternary material.

As reported in the previous section, the methanol electrooxidation on Pt-Ru-Ni catalysts has been extensively investigated. Also if Pt-Ru is not the best binary catalyst for the ethanol oxidation [3], some studies regarding the ethanol electrooxidation on Pt-Ru-Ni catalysts have been carried out [20,77,82,83]. Wang et al. [82,83] studied the effect of Ni addition to Pt-Ru on ethanol oxidation. No significant differences in the onset potential for ethanol electrooxidation on Pt-Ni-Ru/C (6:3:1) and Pt-Ru/C (1:1) were observed: the EOR activity of the Pt-Ru-Ni/C catalyst, however, was higher than that of Pt-Ru/C. As the ECSAs of Pt-Ru-Ni/C and Pt-Ru/C were almost the same, it can be inferred that the SA of Pt-Ru-Ni/C was higher than that of Pt-Ru/C. The high EOR activity of Pt-Ru-Ni was ascribed to hydrogen spillover effect of Ni hydroxides and electronic effect of metallic Ni. A comparison of methanol and ethanol oxidation on Pt-Ru-Ni was carried out by Shen et al. [20]: the  $SA_{Pt-Ru-Ni}/SA_{Pt-Ru}$  ratio for ethanol oxidation was slightly higher than for methanol oxidation. Ribadeneira et al. [77] compared the ethanol oxidation on Pt-Ru-Ni and Pt-Sn-Ni: the  $MA_{Pt-Ru-Ni}/MA_{Pt-Ru}$  ratio for the ethanol oxidation of Pt-Ru-Ni was higher than that of Pt-Sn-Ni. The  $MA_{Pt-Ru-Ni}/MA_{Pt-Ru}$  ratio for the ethanol oxidation of ternary catalysts by different datasets [20,77,82] was higher than that of both P-Ni and Pt-Ru, indicating a synergic effect between Ru and Ni.

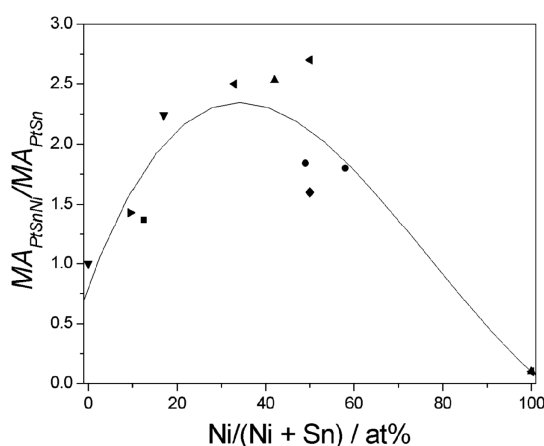


**Figure 7.** Dependence of the Pt-Sn-Ni to Pt-Sn EOR mass activity ( $MA_{Pt-Sn-Ni}/MA_{Pt-Sn}$ ) ratio in acid media on Ni/(Sn + Ni) atomic ratio in Pt-Sn-Ni catalysts with various alloying degrees by different datasets. (▲) Beyhan et al. [50]; (◀) Cantillo et al. [51]; (◆) Parreira et al. [75]; (■) Spinace et al. [76]; (●) Ribadeneira et al. [77]; (▼) Bonesi et al. [78]; (▶) Almeida et al. [80].

## 8. Conclusions

The methanol and ethanol oxidation in acid environment on binary Pt-Ni and ternary Ni-containing Pt-based catalysts has been evaluated on the basis of literature data. Regarding the binary Pt-Ni catalysts, more deeply considerations can be made on the methanol oxidation, due to the higher number of experimental data than those on the ethanol oxidation.

Pt-Ni catalysts presented a MOR activity higher than Pt, but lower than the state-of-the-art Pt-Ru. The lower cost and higher Ni stability in fuel cell environment of nickel than ruthenium, however, make Pt-Ni catalysts promising candidates to substitute Pt-Ru as anode materials in DMFCs. Both specific and mass activities increase with increasing Ni content in the binary catalysts. The SA of PtNi (1:1) catalysts goes to a maximum at an intermediate degree of alloying, corresponding to a Ni content in the alloy of ca. 35 at %, and indicating that the specific activity of a partially alloyed catalysts is higher than that of non-alloyed and fully alloyed catalysts. Regarding the effect of non-alloyed Ni content, at a Pt:Ni atomic ratio in the alloy of 4:1, SA increases with increasing the non-alloyed Ni/Pt atomic ratio by the increase of the amount of NiO, NiOOH, and Ni(OH)<sub>2</sub> species around Pt atoms, facilitating the removal of COads species. However, considering that the ECSA decreases with increasing the amount of Ni oxides, the optimum alloying degree for the mass activity can be different than the optimum alloying degree for the SA. By evaluating the  $I_f/I_b$  ratio, it was inferred that the Pt-Ni electronic interaction dominated the promoting effect of Ni on adsorbed CO oxidation by weakening the Pt-CO bonding energy rather than the bifunctional mechanism related to Ni oxides.

Compared to the MOR, few works reported the ethanol oxidation on Pt-Ni catalysts in acid media, Pt-Ni catalysts presented an EOR activity higher than Pt, but lower than the state-of-the-art Pt-Sn. Both SA and MA increased with increasing Ni content in the catalysts. While taking into account of the few data for the EOR, the slope of  $SA_{Pt-Ni}/SA_{Pt}$  vs. Ni content plot (0.028 at %<sup>-1</sup>) is considerably higher than that for the methanol oxidation (0.010 at %<sup>-1</sup>), indicating that the addition of nickel to Pt is more effective for the EOR than for the MOR. As observed in the case of methanol oxidation, the SA for the ethanol oxidation of Pt-Ni catalysts increases with increasing the non-alloyed Ni content.

Likely, nickel oxide promotes the activation of both the C-H and O-H bonds of ethanol through oxygen-containing species adsorbed on NiO molecules and the change in the density of states near the Fermi level on the Pt surface atoms, but not the C-C bond cleavage.

Regarding the stability of Pt-Ni catalysts, generally, the formation of a Pt skin on the catalyst surface hinders the dissolution of bulk Pt and Ni atoms. A higher stability of the ordered PtNi intermetallic nanoparticles than the disordered PtNi alloy was observed. The Pt<sub>3</sub>Ni<sub>1</sub>/C alloy, due to anchor effects in its structure, showed higher sintering resistance than Pt/C. The mobility of platinum on a carbon surface was hindered in the presence of Ni, thus lowering the sintering rate of Pt atoms.

The addition of Ni to Pt-M (M = Ru, Sn) improves the MOR and EOR activity of the binary catalysts. The MOR activity of Pt-Ru-Ni catalysts has been widely investigated and the MOR activity of Ni-containing catalysts was always higher than that of Pt-Ru. For ternary Pt-M-Ni catalysts, the dependence of the electrochemical parameters on the Ni/(M + Ni) atomic ratio is more interesting than their dependence on the overall Ni content. In the case of methanol oxidation, the  $SA_{Pt-Ru-Ni}/SA_{Pt-Ru}$  vs. Ni/(Ru + Ni) plot presents a sharp peak, followed by a slow decrease of the  $SA_{Pt-Ru-Ni}/SA_{Pt-Ru}$  ratio with increasing Ni content, indicating a synergic effect of Ru and Ni on the MOR specific activity in a short Ni/(Ru + Ni) ratio range, centered at ca. 0.2 Ni/(Ru + Ni). The  $MA_{Pt-Ru-Ni}/MA_{Pt-Ru}/Ni/(Ru + Ni)$  data, instead, are well represented by a parabolic curve with a maximum at ca. 0.45 Ni. The EOR activity of Ni-containing Pt-M-Ni (M = Sn, Ru) catalysts was always higher than that of the parent Pt-M. In the case of Pt-Sn-Ni, a synergic effect between Sn and Ni with a maximum at a value of the Ni/(Sn+Ni) ratio of ca. 0.35 was observed. The presence of Ni in Pt-Sn-Ni catalysts seems to promote C-C bond cleavage and facilitate the removal from the catalyst surface of adsorbed intermediates. The high EOR activity of Pt-Ru-Ni was ascribed to hydrogen spillover effect of Ni hydroxides and electronic effect of metallic Ni.

Future research should be focused on the optimization the total amount of nickel and the relative amount of alloyed and non-alloyed nickel in Pt-Ni catalysts. Indeed, as can be seen in Figure 1a, in the range 0–70 Ni at % for methanol oxidation, and in Figure 4a, in the range 0–40 at % Ni for ethanol oxidation, the specific activity increases with increasing Ni content in Pt-Ni catalyst. However, being the MOR and EOR catalytic activities of Ni alone very poor, optimum values of Ni content for methanol and ethanol oxidation exist and should be evaluated. Also, few studies were addressed to the effect of alloyed and non-alloyed nickel on the catalytic activity of Pt-Ni catalysts. Thus, further investigation on should be carried out to better clarify the effect of alloying degree on methanol and ethanol oxidation. Moreover, to further increase the MOR and EOR activity, the future direction should be the development of unsupported nanostructured Pt-Ni catalysts with high ECSA, such as PtNi nanotubes, nanowires and nanoflowers, and Pt-Ni nanocrystals with well-defined and controllable shape with high SA, such as Pt-Ni nanocubes [84].

**Conflicts of Interest:** The author declares no conflict of interest.

## References

1. Aricò, A.S.; Srinivasan, S.; Antonucci, V. DMFCs: From fundamental aspects to technology development. *Fuel Cells* **2001**, *1*, 133–161. [[CrossRef](#)]
2. Manthiram, A.; Zhao, X.; Li, W. Developments in membranes, catalysts and membrane electrode assemblies for direct methanol fuel cells (DMFCs). *Funct. Mater. Sustain. Energy Appl.* **2012**, *11*, 312–369.
3. Antolini, E. Catalysts for direct ethanol fuel cells. *J. Power Sources* **2007**, *170*, 1–12. [[CrossRef](#)]
4. Badwal, S.P.S.; Giddey, S.; Kulkarni, A.; Goel, J.; Basu, S. Direct ethanol fuel cells for transport and stationary applications—A comprehensive review. *Appl. Energy* **2015**, *145*, 80–103. [[CrossRef](#)]
5. Markovic, N.M.; Gasteiger, H.A.; Ross, P.N.; Jiang, X.; Villegas, I.; Weaver, M.J. Electro-oxidation mechanisms of methanol and formic acid on Pt-Ru alloy surfaces. *Electrochim. Acta* **1995**, *40*, 91–98. [[CrossRef](#)]
6. Gojkovic, S.L.; Vidakovic, T.R.; Durovic, D.R. Kinetic study of methanol oxidation on carbon-supported PtRu electrocatalyst. *Electrochim. Acta* **2003**, *48*, 3607–3614. [[CrossRef](#)]
7. Iwasita, T. Electrocatalysis of methanol oxidation. *Electrochim. Acta* **2002**, *47*, 3663–3674. [[CrossRef](#)]
8. Christensen, P.A.; Hamnett, A.; Troughton, G.L. The role of morphology in the methanol electro-oxidation reaction. *J. Electroanal. Chem.* **1993**, *362*, 207–218. [[CrossRef](#)]
9. Antolini, E. Platinum alloys as anode catalysts for direct methanol fuel cells. In *Electrocatalysis of Direct Methanol Fuel Cells: From Fundamentals to Applications*; Liu, H., Zhang, J., Eds.; Wiley-VCH: Weinheim, Germany, 2009; pp. 227–255.
10. Antolini, E. The problem of Ru dissolution from Pt–Ru catalysts during fuel cell operation: Analysis and solutions. *J. Solid State Electrochem.* **2011**, *15*, 455–472. [[CrossRef](#)]
11. Zignani, S.C.; Baglio, V.; Linares, J.J.; Monforte, G.; Gonzalez, E.R.; Aricò, A.S. Endurance study of a solid polymer electrolyte direct ethanol fuel cell based on a Pt–Sn anode catalyst. *Int. J. Hydrogen Energy* **2013**, *38*, 11576–11582. [[CrossRef](#)]
12. Park, K.-W.; Choi, J.-H.; Kwon, B.-K.; Lee, S.-A.; Sung, Y.-E.; Ha, H.-Y.; Hong, S.-A.; Kim, H.; Wieckowski, A. Chemical and electronic effects of Ni in Pt/Ni and Pt/Ru/Ni alloy nanoparticles in methanol electrooxidation. *J. Phys. Chem. B* **2002**, *106*, 1869–1877. [[CrossRef](#)]
13. Lu, X.-G.; Sundman, B. Thermodynamic assessments of the Ni-Pt and Al-Ni-Pt systems. *Calphad* **2009**, *33*, 450–456. [[CrossRef](#)]
14. Staunton, J.; Weinberger, P.; Gyorffy, B.L. On the electronic structure of paramagnetic Ni<sub>c</sub>Pt<sub>1-c</sub> alloys: A relativistic calculation. *J. Phys. F Met. Phys.* **1983**, *13*, 779–786. [[CrossRef](#)]
15. De Temmerman, L.; Creemers, C.; Van Hove, H.; Neyens, A.; Bertolini, J.C.; Massardier, J. Experimental determination of equilibrium surface segregation in Pt-Ni single crystal alloys. *Surf. Sci.* **1986**, *178*, 888–896. [[CrossRef](#)]
16. Wang, G.; Van Hove, M.A.; Ross, P.N.; Baskes, M.I. Quantitative prediction of surface segregation in bimetallic Pt–M alloy nanoparticles (M = Ni, Re, Mo). *Prog. Surf. Sci.* **2005**, *79*, 28–45. [[CrossRef](#)]

17. Stamenkovic, V.; Schmidt, T.J.; Ross, P.N.; Markovic, N.M. Surface composition effect in electrocatalysis: Kinetics of oxygen reduction on well-defined Pt<sub>3</sub>Ni and Pt<sub>3</sub>Co alloy surfaces. *J. Phys. Chem. B* **2002**, *106*, 11970–11979. [[CrossRef](#)]
18. Park, K.W.; Choi, J.H.; Sung, Y.E. Structural, chemical, and electronic properties of Pt/Ni thin film electrodes for methanol electrooxidation. *J. Phys. Chem. B* **2003**, *107*, 5851–5856. [[CrossRef](#)]
19. Page, T.; Johnson, R.; Hormes, J.; Noding, S.; Rambabu, B. A study of methanol electro-oxidation reactions in carbon membrane electrodes and structural properties of Pt alloy electro-catalysts by EXAFS. *J. Electroanal. Chem.* **2000**, *485*, 34–41. [[CrossRef](#)]
20. Shen, Y.; Xiao, K.; Xi, J.; Qiu, X. Comparison study of few-layered graphene supported platinum and platinum alloys for methanol and ethanol electro-oxidation. *J. Power Sources* **2015**, *278*, 235–244. [[CrossRef](#)]
21. Zhou, Y.-Y.; Liu, C.-H.; Liu, J.; Cai, X.-L.; Lu, Y.; Zhang, H.; Sun, X.-H.; Wang, S.-D. Self-decoration of PtNi alloy nanoparticles on multiwalled carbon nanotubes for highly efficient methanol electro-oxidation. *Nano-Micro Lett.* **2016**, *8*, 371–380. [[CrossRef](#)]
22. Agrawal, A.K.; Rangarajan, J. Electro-catalytic activity of nano-sized Pt-Ni bimetallic alloy particles supported on carbon for methanol electro-oxidation. *Int. J. Sci. Eng. Res.* **2014**, *5*, 1544–1551.
23. Amin, R.S.; Abdel Hameed, R.M.; El-Khatib, K.M.; Youssef, M.E.; Elzatahry, A.A. Pt–NiO/C anode electrocatalysts for direct methanol fuel cells. *Electrochim. Acta* **2012**, *59*, 499–508. [[CrossRef](#)]
24. Nagashree, K.L.; Raviraj, N.H.; Ahmed, M.F. Carbon paste electrodes modified by Pt and Pt–Ni microparticles dispersed in polyindole film for electrocatalytic oxidation of methanol. *Electrochim. Acta* **2010**, *55*, 2629–2635. [[CrossRef](#)]
25. Zhao, Y.; Yifeng, E.; Fan, L.; Qiu, Y.; Yang, S. A new route for the electrodeposition of platinum–nickel alloy nanoparticles on multi-walled carbon nanotubes. *Electrochim. Acta* **2007**, *52*, 5873–5878. [[CrossRef](#)]
26. Zhao, Y.; Fan, L.; Ren, J.; Hong, B. Electrodeposition of Pt–Ru and Pt–Ru–Ni nanoclusters on multi-walled carbon nanotubes for direct methanol fuel cell. *Int. J. Hydrogen Energy* **2014**, *39*, 4544–4557. [[CrossRef](#)]
27. Hsieh, C.-T.; Lin, J.-Y. Fabrication of bimetallic Pt–M (M = Fe, Co, and Ni) nanoparticle/carbon nanotube electrocatalysts for direct methanol fuel cells. *J. Power Sources* **2009**, *188*, 347–352. [[CrossRef](#)]
28. Antolini, A.; Salgado, J.R.C.; Gonzalez, E.R. Oxygen reduction on a Pt<sub>70</sub>Ni<sub>30</sub>/C electrocatalyst prepared by the borohydride method in H<sub>2</sub>SO<sub>4</sub>/CH<sub>3</sub>OH solutions. *J. Power Sources* **2006**, *155*, 161–166. [[CrossRef](#)]
29. Yang, H.; Coutanceau, C.; Léger, J.-M.; Alonso-Vante, N.; Lamy, C. Methanol tolerant oxygen reduction on carbon-supported Pt–Ni alloy nanoparticles. *J. Electroanal. Chem.* **2005**, *576*, 305–313. [[CrossRef](#)]
30. Drillet, J.-F.; Ee, A.; Friedemann, J.; Kötz, R.; Schnyder, B.; Schmidt, V.M. Oxygen reduction at Pt and Pt<sub>70</sub>Ni<sub>30</sub> in H<sub>2</sub>SO<sub>4</sub>/CH<sub>3</sub>OH solution. *Electrochim. Acta* **2002**, *47*, 1983–1988. [[CrossRef](#)]
31. Antolini, E.; Salgado, J.R.C.; Gonzalez, E.R. The methanol oxidation reaction on platinum alloys with the first row transition metals: The case of Pt–Co and –Ni alloy electrocatalysts for DMFCs: A short review. *Appl. Catal. B Environ.* **2006**, *63*, 137–149. [[CrossRef](#)]
32. Manoharan, R.; Goodenough, J.B. Methanol oxidation in acid on ordered NiTi. *J. Mater. Chem.* **1992**, *2*, 875–887. [[CrossRef](#)]
33. Habibi, B.; Dadashpour, E. Carbon-ceramic supported bimetallic PtNi nanoparticles as an electrocatalyst for electrooxidation of methanol and ethanol in acidic media. *Int. J. Hydrogen Energy* **2013**, *38*, 5425–5434. [[CrossRef](#)]
34. Guo, W.; Tian, W.Q.; Lian, X.; Liu, F.; Zhou, M.; Xiao, P.; Zhang, Y. A comparison of the dominant pathways for the methanol dehydrogenation to CO on Pt<sub>7</sub> and Pt<sub>7–x</sub>Ni<sub>x</sub> (x = 1, 2, 3) bimetallic clusters: A DFT study. *Comput. Theor. Chem.* **2014**, *1032*, 73–83. [[CrossRef](#)]
35. Xu, C.; Hou, J.; Pang, X.; Li, X.; Zhu, M.; Tang, B. Nanoporous PtCo and PtNi alloy ribbons for methanol electrooxidation. *Int. J. Hydrogen Energy* **2012**, *37*, 10489–10498. [[CrossRef](#)]
36. Stamenkovic, V.; Mun, B.S.; Mayrhofer, K.J.; Ross, P.N.; Markovic, N.M.; Rossmeisl, J.; Greeley, J.; Norskov, J.K. Changing the activity of electrocatalysts for oxygen reduction by tuning the surface electronic structure. *Angew. Chem. Int. Ed.* **2006**, *45*, 2897–2901. [[CrossRef](#)] [[PubMed](#)]
37. Wang, L.-L.; Zhang, D.-F.; Guo, L. Phase-segregated Pt–Ni chain-like nanohybrids with high electrocatalytic activity towards methanol oxidation reaction. *Nanoscale* **2014**, *6*, 4635–4641. [[CrossRef](#)] [[PubMed](#)]
38. Jiang, S.; Ma, Y.; Tao, H.; Jian, G.; Wang, X.; Fan, Y.; Zhu, J.; Hu, Z. Highly dispersed Pt–Ni nanoparticles on nitrogen-doped carbon nanotubes for application in direct methanol fuel cells. *J. Nanosci. Nanotechnol.* **2010**, *10*, 3895–3900. [[CrossRef](#)] [[PubMed](#)]

39. Nassr, A.B.A.A.; Sinev, I.; Grünert, W.; Bron, M. PtNi supported on oxygen functionalized carbon nanotubes: In depth structural characterization and activity for methanol electrooxidation. *Appl. Catal. B Environ.* **2013**, *142–143*, 849–860. [[CrossRef](#)]
40. Hao, Y.; Wang, X.; Zheng, Y.; Shen, J.; Yuan, J.; Wang, A.; Niu, L.; Huang, S. Size-controllable synthesis of ultrafine PtNi nanoparticles uniformly deposited on reduced graphene oxide as advanced anode catalysts for methanol oxidation. *Int. J. Hydrogen Energy* **2016**, *41*, 9303–9311. [[CrossRef](#)]
41. Wang, Y.; Zang, J.; Dong, L.; Pan, H.; Yuan, Y.; Wang, Y. Graphitized nanodiamond supporting PtNi alloy as stable anodic and cathodic electrocatalysts for direct methanol fuel cell. *Electrochim. Acta* **2013**, *113*, 583–590. [[CrossRef](#)]
42. Luo, B.; Xu, S.; Yan, X.; Xue, Q. PtNi alloy nanoparticles supported on polyelectrolyte functionalized graphene as effective electrocatalysts for methanol oxidation. *J. Electrochem. Soc.* **2013**, *160*, F262–F268. [[CrossRef](#)]
43. Hu, Y.; Wu, P.; Yin, Y.; Zhang, H.; Cai, C. Effects of structure, composition, and carbon support properties on the electrocatalytic activity of Pt-Ni-graphene nanocatalysts for the methanol oxidation. *Appl. Catal. B Environ.* **2012**, *111–112*, 208–217. [[CrossRef](#)]
44. Zhou, X.-W.; Zhang, R.-H.; Zhou, Z.-Y.; Sun, S.-G. Preparation of PtNi hollow nanospheres for the electrocatalytic oxidation of methanol. *J. Power Sources* **2011**, *196*, 5844–5848. [[CrossRef](#)]
45. Yang, H.; Vogel, W.; Lamy, C.; Alonso-Vante, N. Structure and electrocatalytic activity of carbon-supported Pt-Ni alloy nanoparticles toward the oxygen reduction reaction. *J. Phys. Chem. B* **2004**, *108*, 11024–11034. [[CrossRef](#)]
46. Comignani, V.; Sieben, J.M.; Brigante, M.E.; Duarte, M.M. Carbon supported Pt-NiO nanoparticles for ethanol electro-oxidation in acid media. *J. Power Sources* **2015**, *278*, 119–127. [[CrossRef](#)]
47. Li, L.; Wu, Y.; Lu, J.; Nan, C.; Li, Y. Synthesis of Pt-Ni-graphene *via in situ* reduction and its enhanced catalyst activity for the methanol oxidation. *Chem. Commun.* **2013**, *49*, 7486–7488. [[CrossRef](#)] [[PubMed](#)]
48. Antolini, E.; Salgado, J.R.C.; dos Santos, A.M.; Gonzalez, E.R. Carbon-supported Pt-Ni alloys prepared by the borohydride method as electrocatalysts for DMFCs. *Electrochem Solid-State Lett.* **2005**, *8*, A226–A230. [[CrossRef](#)]
49. Wang, X.; Wang, H.; Lei, Z.; Zhang, Z.; Wang, R. The performance of carbon-supported platinum-decorated nickel electrocatalyst for ethanol oxidation. *Chin. J. Catal.* **2011**, *32*, 1519–1524. [[CrossRef](#)]
50. Beyhan, S.; Léger, J.-M.; Kadirgan, F. Pronounced synergetic effect of the nano-sized PtSnNi/C catalyst for ethanol oxidation in direct ethanol fuel cell. *Appl. Catal. B Environ.* **2013**, *130–131*, 305–313. [[CrossRef](#)]
51. Cantillo, N.M.; Solla-Gullon, J.; Herrero, E.; Sanchez, C. Ethanol electrooxidation on PtSnNi/C nanoparticles prepared in water-in-oil microemulsion. *ECS Trans.* **2011**, *41*, 1307–1316.
52. Ponmani, K.; Kiruthika, S.; Muthukumar, B. Investigation of nanometals (Ni and Sn) in platinum-based ternary electrocatalysts for ethanol electro-oxidation in membraneless fuel cells. *J. Electrochem. Sci. Technol.* **2015**, *6*, 95–105. [[CrossRef](#)]
53. Greeley, J.; Nørskov, J.K. Electrochemical dissolution of surface alloys in acids: Thermodynamic trends from first-principles calculations. *Electrochim. Acta* **2007**, *52*, 5829–5836. [[CrossRef](#)]
54. Bonakdarpour, A.; Wenzel, J.; Stevens, D.A.; Sheng, S.; Monchesky, T.L.; Lobel, R.; Atanasoski, R.T.; Schmoeckel, A.K.; Vernstrom, G.D.; Debe, M.K.; et al. Studies of transition metal dissolution from combinatorially sputtered, nanostructured Pt<sub>1-x</sub>M<sub>x</sub> (M = Fe, Ni; 0 < x < 1) electrocatalysts for PEM fuel cells. *J. Electrochem. Soc.* **2005**, *152*, A61–A72.
55. Hoshi, Y.; Yoshida, T.; Nishikata, A.; Tsuru, T. Dissolution of Pt-M (M: Cu, Co, Ni, Fe) binary alloys in sulfuric acid solution. *Electrochim. Acta* **2011**, *56*, 5302–5309. [[CrossRef](#)]
56. Colón-Mercado, H.R.; Kim, H.; Popov, B.N. Durability study of Pt<sub>3</sub>Ni<sub>1</sub> catalysts as cathode in PEM fuel cells. *Electrochem. Commun.* **2004**, *6*, 795–799. [[CrossRef](#)]
57. Colón-Mercado, H.R.; Popov, B.N. Stability of platinum based alloy cathode catalysts in PEM fuel cells. *J. Power Sources* **2006**, *155*, 253–263. [[CrossRef](#)]
58. Zignani, S.C.; Antolini, E.; Gonzalez, E.R. Stability of Pt-Ni/C (1:1) and Pt/C electrocatalysts as cathode materials for polymer electrolyte fuel cells: Effect of ageing tests. *J. Power Sources* **2009**, *191*, 344–350. [[CrossRef](#)]
59. Borup, R.L.; Davey, J.R.; Garzon, F.H.; Wood, D.L.; Inbody, M.A. PEM fuel cell electrocatalyst durability measurements. *J. Power Sources* **2006**, *163*, 76–81. [[CrossRef](#)]

60. Watanabe, M.; Tsurumi, K.; Mizukami, T.; Nakamura, T.; Stonehart, P. Activity and stability of ordered and disordered Co-Pt alloys for phosphoric acid fuel cells. *J. Electrochem. Soc.* **1994**, *141*, 2659–2668. [[CrossRef](#)]
61. Zou, L.; Li, J.; Yuan, T.; Zhou, Y.; Li, X.; Yang, H. Structural transformation of carbon-supported PtCr nanoparticles from a disordered to an ordered phase as a durable oxygen reduction electrocatalyst. *Nanoscale* **2014**, *6*, 10686–10692. [[CrossRef](#)] [[PubMed](#)]
62. Antolini, E. Platinum-based ternary catalysts for low temperature fuel cells: Part I. Preparation methods and structural characteristics. *Appl. Catal. B Environ.* **2007**, *74*, 324–336. [[CrossRef](#)]
63. Huang, T.; Liu, J.; Li, R.; Cai, W.; Yu, A. A novel route for preparation of PtRuMe (Me = Fe, Co, Ni) and their catalytic performance for methanol electrooxidation. *Electrochem. Commun.* **2009**, *11*, 643–646. [[CrossRef](#)]
64. Jeon, M.K.; Lee, K.R.; Daimon, H.; Nakahara, A.; Woo, S.I. Pt<sub>45</sub>Ru<sub>45</sub>M<sub>10</sub>/C (M = Fe, Co, and Ni) catalysts for methanol electro-oxidation. *Catal. Today* **2008**, *132*, 123–126. [[CrossRef](#)]
65. Kang, D.K.; Noh, C.S.; Kim, N.H.; Cho, S.-H.; Sohn, J.M.; Kim, T.J.; Park, Y.-K. Effect of transition metals (Ni, Sn and Mo) in Pt<sub>5</sub>Ru<sub>4</sub>M alloy ternary electrocatalyst on methanol electro-oxidation. *J. Ind. Eng. Chem.* **2010**, *16*, 385–389. [[CrossRef](#)]
66. Papaderakis, A.; Pliatsikas, N.; Prochaska, C.; Papazisi, K.M.; Balomenou, S.P.; Tsiplakides, D.; Patsalas, P.; Sotiropoulos, S. Ternary Pt-Ru-Ni catalytic layers for methanol electrooxidation prepared by electrodeposition and galvanic replacement. *Front. Chem.* **2014**, *2*, 29. [[CrossRef](#)] [[PubMed](#)]
67. Liu, J.; Cao, J.; Huang, Q.; Li, X.; Zou, Z.; Yang, H. Methanol oxidation on carbon-supported Pt-Ru-Ni ternary nanoparticle electrocatalysts. *J. Power Sources* **2008**, *175*, 159–165. [[CrossRef](#)]
68. Wang, Z.B.; Yin, G.P.; Shi, P.F.; Sun, Y.C. Novel Pt-Ru-Ni/C catalysts for methanol electro-oxidation in acid medium. *Electrochem. Solid-State Lett.* **2006**, *9*, A13–A15. [[CrossRef](#)]
69. Martínez-Huerta, M.V.; Rojas, S.; Gomez de la Fuente, J.L.; Terreros, P.; Peña, M.A.; Fierro, J.L.G. Effect of Ni addition over PtRu/C based electrocatalysts for fuel cell applications. *Appl. Catal. B Environ.* **2006**, *69*, 75–84. [[CrossRef](#)]
70. Ye, F.; Chen, S.; Dong, X.; Lin, W. Carbon nanotubes supported Pt-Ru-Ni as methanol electro-oxidation catalyst for direct methanol fuel cells. *J. Nat. Gas Chem.* **2007**, *16*, 162–166. [[CrossRef](#)]
71. Zhao, J.; Li, H.; Liu, Z.; Hu, W.; Zhao, C.; Shi, D. An advanced electrocatalyst with exceptional electrocatalytic activity via ultrafine Pt-based trimetallic nanoparticles on pristine grapheme. *Carbon* **2015**, *87*, 116–127. [[CrossRef](#)]
72. Cheng, Y.; Shen, P.K.; Jiang, S.P. Enhanced activity and stability of core-shell structured PtRuNi<sub>x</sub> electrocatalysts for direct methanol fuel cells. *Int. J. Hydrogen Energy* **2016**, *41*, 1935–1943. [[CrossRef](#)]
73. Antolini, E.; Gonzalez, E.R. Effect of synthesis method and structural characteristics of Pt-Sn fuel cell catalysts on the electro-oxidation of CH<sub>3</sub>OH and CH<sub>3</sub>CH<sub>2</sub>OH in acid medium. *Catal. Today* **2011**, *160*, 28–38. [[CrossRef](#)]
74. Beyhan, S.; Coutanceau, C.; Léger, J.-M.; Napporn, T.W.; Kadırgan, F. Promising anode candidates for direct ethanol fuel cell: Carbon supported PtSn-based trimetallic catalysts prepared by Bönemann method. *Int. J. Hydrogen Energy* **2013**, *38*, 6830–6841. [[CrossRef](#)]
75. Parreira, L.S.; da Silva, J.C.M.; D’Villa-Silva, M.; Simões, F.C.; Garcia, S.; Gaubeur, I.; Cordeiro, M.A.L.; Leite, E.R.; dos Santos, M.C. PtSnNi/C nanoparticle electrocatalysts for the ethanol oxidation reaction: Ni stability study. *Electrochim. Acta* **2013**, *96*, 243–252. [[CrossRef](#)]
76. Spinacé, E.V.; Linardi, M.; Oliveira Neto, A. Co-catalytic effect of nickel in the electro-oxidation of ethanol on binary Pt-Sn electrocatalysts. *Electrochem. Commun.* **2005**, *7*, 365–369. [[CrossRef](#)]
77. Ribadeneira, E.; Hoyos, B.A. Evaluation of Pt-Ru-Ni and Pt-Sn-Ni catalysts as anodes in direct ethanol fuel cells. *J. Power Sources* **2008**, *180*, 238–242. [[CrossRef](#)]
78. Bonesi, A.; Garaventa, G.; Triaca, W.E.; Castro Luna, A.M. Synthesis and characterization of new electrocatalysts for ethanol oxidation. *Int. J. Hydrogen Energy* **2008**, *33*, 3499–3501. [[CrossRef](#)]
79. Bonesi, A.R.; Moreno, M.S.; Triaca, W.E.; Castro Luna, A.M. Modified catalytic materials for ethanol oxidation. *Int. J. Hydrogen Energy* **2010**, *35*, 5999–6004. [[CrossRef](#)]
80. Almeida, T.S.; Van Wassen, A.R.; VanDover, R.B.; de Andrade, A.R.; Abruña, H.D. Combinatorial PtSnM (M = Fe, Ni, Ru and Pd) nanoparticle catalyst library toward ethanol electrooxidation. *J. Power Sources* **2015**, *284*, 623–630. [[CrossRef](#)]

81. Beyhan, S.; Léger, J.-M.; Kadirgan, F. Understanding the influence of Ni, Co, Rh and Pd addition to PtSn/C catalyst for the oxidation of ethanol by in situ Fourier transform infrared spectroscopy. *Appl. Catal. B Environ.* **2014**, *144*, 66–74. [[CrossRef](#)]
82. Wang, Z.-B.; Yin, G.-P.; Zhang, J.; Sun, Y.-C.; Shi, P.-F. Investigation of ethanol electrooxidation on a Pt–Ru–Ni/C catalyst for a direct ethanol fuel cell. *J. Power Sources* **2006**, *160*, 37–43. [[CrossRef](#)]
83. Wang, Z.-B.; Zuo, P.-J.; Wang, G.-J.; Du, C.-Y.; Yin, G.-P. Effect of Ni on PtRu/C catalyst performance for ethanol electrooxidation in acidic medium. *J. Phys. Chem. C* **2008**, *112*, 6582–6587. [[CrossRef](#)]
84. Antolini, E.; Perez, J. The renaissance of unsupported nanostructured catalysts for low-temperature fuel cells: From the size to the shape of metal nanostructures. *J. Mater. Sci.* **2011**, *46*, 4435–4457. [[CrossRef](#)]



© 2017 by the author; licensee MDPI, Basel, Switzerland. This article is an open access article distributed under the terms and conditions of the Creative Commons Attribution (CC-BY) license (<http://creativecommons.org/licenses/by/4.0/>).